SCALAR MIXING IN AXISYMMETRIC JETS WITH EXTERNAL TURBULENCE

Khashayar F. Kohan† **and Susan J. Gaskin**‡
Department of Civil Engineering, McGill University, Montréal, Québec, H3A 0C3, Canada
†khashayar.feizbakhshiankohan@mail.mcgill.ca, ‡susan.gaskin@mcgill.ca

ABSTRACT

The present study aims to understand the process of turbulent entrainment into a jet, as affected by background turbulence, using scalar statistics. Planar-laser-induced fluorescence was employed to capture the orthogonal cross sections of the jet at a fixed downstream station with varying background turbulence intensities and length scales. The conditional scalar profiles revealed that the thickness of the scalar turbulent/turbulent interface (TTI) is greater than that of the traditional turbulent/non-turbulent interface (TNTI), and the interfacial thickness is an increasing function of the background turbulence intensity. Although nibbling remains the primary entrainment mechanism in the far field, increased occurrence of concentration 'holes' within the interfacial layer in the presence of ambient turbulence suggests a more significant role of large-scale engulfment in the turbulent/turbulent entrainment paradigm. Enhanced contribution of the area of detached scalar patches ('islands') to that of the main jet is hypothesized to be evidence of intense detrainment events in the background turbulence. This can potentially explain the reduced net entrainment into the jet, which manifests as less negative values of scalar skewness within the jet core.

INTRODUCTION

Turbulent entrainment refers to the spatio-temporal process by which the ambient fluid, whether irrotational or turbulent, is incorporated into the primary turbulent flow. Conversely, detrainment signifies the transfer of fluid from the primary turbulent flow back into the ambient. The mechanisms of entrainment, i.e., small-scale viscous/molecular nibbling and large-scale inviscid engulfment, have been studied to a great extent in several turbulent flows in a non-turbulent (quiescent) ambient. It is generally understood that the nibbling mechanism dominates that of engulfment in unperturbed free-shear flows (e.g. Westerweel *et al.* 2009; Jahanbakhshi & Madnia 2016). The properties of the outer layer of turbulent flows in the quiescent ambient, termed the turbulent/non-turbulent interface (TNTI), are also well studied; for a thorough review see da Silva *et al.* (2014*a*).

Whilst the behaviour of the TNTI is well established, relatively few studies have examined the characteristics of the interfacial layer between a turbulent ambient and a turbulent flow, that is, the turbulent/turbulent interface (TTI). The mean effect of background turbulence is to enhance the large- and small-scale undulations of the interface, in what seems to be a universal outcome in wall-bounded (You & Zaki 2019) and free-shear flows (Kankanwadi & Buxton 2020; Kohan & Gaskin 2022). In other words, the TTI outline is on average rougher than that of the TNTI, where 'outline' henceforth denotes the outer boundary of the TNTI and TTI. It is essential to note that albeit thin, the TNTI and TTI have finite thickness, across which the vorticity and scalar adjust between the ambient and the primary turbulent flow.

The presence of external forcing (e.g. turbulence or stratification) may change the basic flow structure, and, therefore, the balance between the entrainment mechanisms. Westerweel *et al.* (2009) postulated the dominance of engulfment/detrainment over nibbling in free-shear flows exposed to strong external forcing. Intermittent detrainment events have been observed in experiments involving filling-box plumes attached to a vertical wall and subjected to sufficiently strong ambient stratification. This phenomenon, termed 'plume peeling', manifests as intrusions of passive scalar patches originating from the plume into the environment (e.g. Gladstone & Woods 2014). An increased occurrence of detrainment events was also qualitatively demonstrated for boundary layers in external turbulence relative to a non-turbulent ambient (You & Zaki 2019), consistent with our visualizations in figure 1.

The effect of background turbulence on the entrainment process in the far field of a jet is three-fold in the sense that it acts (i) to increase the surface area across which entrainment occurs (see e.g. figure 1), (ii) to break up the coherent structures of the jet, thereby reducing the mean axial velocity and the induced entrainment wind (Hunt 1994; Khorsandi *et al.* 2013), and (iii) to promote large detrainment events as compared to the non-turbulent background. It is generally understood that the second and third effects dominate the former, and, thus, the rate of entrainment is suppressed in a turbulent ambient (Hunt 1994; Gaskin *et al.* 2004; Khorsandi *et al.* 2013; Sahebjam *et al.* 2022). Eventually, the turbulent ambient breaks up the jet at a critical background turbulence intensity. For example, in a zero-mean-flow approximately homogeneous background turbulence generated by a random jet array (RJA), the onset of break-up for an axisymmetric jet occurs once $\xi = u_\tau/u^{rms}_{jet,q} > 0.5$ (Sahebjam *et al.* 2022), where ξ, u_τ, and $u^{rms}_{jet,q}$ denote the relative turbulence intensity between the ambient and the jet, the characteristic velocity of the ambient turbulence, and streamwise (x) root-mean-square (r.m.s.) velocity at the jet centerline in the quiescent ambient, respectively. The jet-driven entrainment halts beyond the break-up point, and the TTI outline diffuses like a passive interface in the turbulent ambient. In light of these observations, however, it becomes evident that understanding of the impact of external turbulence on the relative importance of different entrainment mechanisms into the jet is still lacking.

Our intention is to provide new insights on the interplay between nibbling, engulfment, and detrainment of jets in external turbulence. Hence, in the present study, we investigate the interfacial and entrainment processes in the far field of an

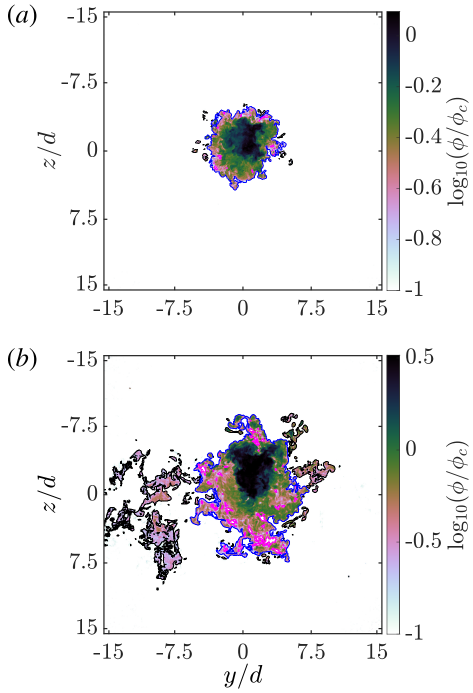

Figure 1. Normalized instantaneous scalar fields (ϕ/ϕ_c) of an axisymmetric jet in (*a*) quiescent ambient (case Q) and in (*b*) turbulent ambient (case T3) in logarithmic scaling. Here, ϕ_c represents the ensemble-averaged centerline concentration. The TNTI and TTI outlines, ambient 'holes', and apparently detached 'islands' are shown with the blue, magenta, and black lines, respectively.

axisymmetric jet subjected to RJA-generated turbulence, using scalar statistics.

METHODOLOGY

The planar laser-induced fluorescence (PLIF) measurements were carried out in a $1.5 \times 6 \times 1\,\mathrm{m}^3$ open-top glass tank with walls of tempered glass to provide optical access. A 12-bit, 4 MP CMOS camera (pco.dimax) was used at a sampling frequency of 50 Hz to capture the scalar field in orthogonal cross sections of a round jet at a downstream station of $x/d = 25$, having a Reynolds number of $Re_J = 10600$ based on its diameter (d) and exit velocity. The field of view (FOV), spanning a region of $260 \times 260\,\mathrm{mm}^2$, was illuminated by a 1.5 mm thick laser sheet, which was formed by an 8-sided polygonal rotating mirror. In order for the scalar to faithfully track the jet fluid (water), a high-Schmidt number ($Sc \gg 1$) passive scalar was used, namely, Rhodamine 6G with $Sc \approx 2500$. The current PLIF resolution (assessed as ≈ 1.7 centerline Kolmogorov microscale in the quiescent ambient, η_q) is sufficient to capture the conditional scalar statistics relative to the location of the outline (Kohan & Gaskin 2020), which is required to estimate the thickness of the interfacial layers. The jet-centerline values of the Kolmogorov and Taylor (λ_q) microscales in the quiescent ambient are calculated from the empirical relations of Friehe *et al.* (1971),

$$\eta_q/d = (48Re_J^3)^{-1/4}(x/d), \quad \lambda_q/d = 0.88Re_J^{-1/2}(x/d). \tag{1a,b}$$

A systematic study was conducted to elicit the effect of increasing background turbulence intensity on the properties of the interfacial layer and the entrainment process. We note that the length scale of the ambient turbulence, l_τ, is relatively unimportant in characterizing the behaviour of the interfacial layer in the far field (Kankanwadi & Buxton 2020; Kohan & Gaskin 2022). Nonetheless, figure 2(*a*) presents the relative turbulence intensity, $\xi = u_\tau/u_{jet,q}^{rms}$, and length scale, $\mathscr{L} = l_\tau/b_{\phi,q}$, between the ambient and the jet for the studied cases, where $b_{\phi,q}$ represents the concentration half-width of the reference case, that is, the jet in a quiescent background (case Q). The other runs in this experimental campaign are named such that the prefix (case <u>T</u>#) denotes the jet in the turbulent ambient, while the hierarchical order of the suffix (case T<u>#</u>) reflects the increasing background turbulence intensity. Further details on the calculation of ξ and $\mathscr{L}$ can be found in Kohan & Gaskin (2022).

The characteristics (i.e. u_τ and l_τ) of the zero-mean-flow external turbulence were controlled by moving the RJA sheet relative to the jet exit (along the y-axis); the closer the RJA to the jet, the more intense the background turbulence. The RJA comprised 60 bilge pumps with center-to-center distance of $M = 15$ cm (figure 2*b*). The optimized 'random' algorithm driving the RJA, generated an approximately homogeneous turbulence across the average width of the jet for the cases considered here. In other words, the unavoidable decay of the RJA-generated turbulence does not systematically influence the behaviour of the jet across its width, and, thus, averaging the scalar statistics over the TTI outline length is considered appropriate (Kohan & Gaskin 2022).

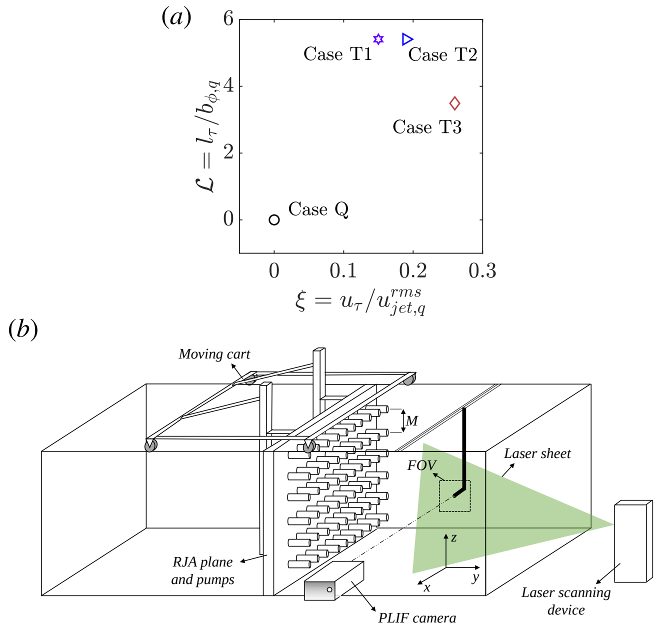

Figure 2. (*a*) Experimental envelope presenting the relative turbulence intensity and length scale of the conducted cases. (*b*) An illustration of the experimental set-up.

RESULTS

Scaling of the Scalar TNTI and TTI

The identification of the TNTI and TTI outlines is performed by placing a threshold, ϕ_t, on the instantaneous scalar concentration fields, noting that $0.11 \leqslant \phi_t/\phi_c \leqslant 0.14$ for the cases considered herein. Thereafter, the conditional profiles (denoted by $\langle\sim\rangle_I$) are assessed as ensemble-averaged flow variables (i.e. mean and r.m.s. concentration) along the local interface-normal coordinate, represented by x_n. Note that $x_n > 0$ and $x_n < 0$ point into the jet and into the ambient, respectively, while $x_n = 0$ lies on the outline.

The existence of the scalar TTI was first verified in Kohan & Gaskin (2022) with the evidence reproduced here in the form of figure 3(*a*). This figure reports the behaviour of conditional mean scalar relative to the position of the outline, $\langle\phi\rangle_I$, exhibiting sharp jumps across the TTI layers akin to the classical TNTI. It is also evident that the value of the conditional jump monotonically increases with ξ. This suggests the possibility of enhanced transport of concentration from the jet core towards the edges in background turbulence, causing greater levels of passive scalar to exist within the interfacial layer.

Additional insight regarding the concentration transport near the outline may be obtained by considering the two-point scalar correlation in the interface-normal frame of reference. Figure 3(*b*) depicts the concentration cross-correlation,

$$C_{\phi\phi}(x_r,\delta) = \frac{\langle\phi'(x_r)\phi'(x_r+\delta)\rangle_I}{\langle\phi^{rms}(x_r)\rangle_I\langle\phi^{rms}(x_r+\delta)\rangle_I}, \qquad (2)$$

with the reference point, x_r, situated within the finite thickness of the scalar interfacial layer at $x_n/b_\phi = 0.025$ for all cases. Note that this point is clearly located within the region characterized by the sharp jump/discontinuity in mean concentration (the dashed-dotted line in figure 3*a*). We also checked that small modifications of the reference point location do not alter the results. Here, δ denotes the lag distance along the interface-normal coordinate, moving into the jet region. The stronger correlation observed between the passive scalar values in the interfacial layer and the core reaffirms the notion of enhanced transport in background turbulence. This is attributed to increased turbulent diffusion and mean radial velocities at the edges of the jet in external turbulence, as shown by the velocity measurements of Khorsandi *et al.* (2013).

The thickness of the scalar interfacial layers can be estimated by exploiting the quasi-step jump in the profiles of $\langle\phi\rangle_I$. In particular, the thickness of the scalar TNTI and TTI layers is evaluated by applying a threshold to the gradient of the conditional concentration, $\langle\phi\rangle_I' = \mathrm{d}\langle\phi\rangle_I/\mathrm{d}x_n$ (figures 3*c*,*d*). The threshold is defined as $\langle\phi\rangle_I' = \zeta[\langle\phi\rangle_I']_{max}$, noting that the results presented herein are largely insensitive to the specific choice of ζ for $\zeta \in [0.09, 0.9]$. Subsequently, the extent of the interfacial layer is calculated as the distance between $x_n = 0$ (i.e. the outline) and the intersection of $\langle\phi\rangle_I'/[\langle\phi\rangle_I']_{max}$ and the selected threshold. Figure 3(*c*) reveals that the absolute values of the interfacial thickness follow the hierarchy of ξ, that is, the adjustment of passive scalar between the jet and the ambient is delayed due to the presence of external turbulence. Figure 3(*d*) presents the same data as figure 3(*c*), with the difference being that the interface-normal coordinate is normalized by the local concentration half-width; a potentially relevant length scale. It is again evident that background turbulence acts to widen the extent of the scalar interfacial layer at the edges of the jet relative to a non-turbulent ambient, while cases with external turbulence exhibit a reasonable degree of collapse. It is also worthwhile mentioning that a value of $\zeta = \mathcal{O}(0.1)$ has been utilized in a number of studies to estimate the thickness of the scalar interfacial layer (e.g. Wu *et al.* 2019). The inset of figure 3(*d*) shows that upon employing $\zeta = 0.1 \sim 0.2$, a value of $\mathcal{O}(10\eta_q)$ or $\mathcal{O}(\lambda_q)$ is recovered as the thickness of the scalar adjustment region for the cases studied herein, which is in line with previous experiments on the scalar interfacial layer (e.g. Kohan & Gaskin 2020).

Entrainment/Detrainment Analysis

The concentration holes (also referred to as bubbles) represent regions with $\phi < \phi_t$ that lie within the jet. Only holes with an area, A_h, greater than 4 pixels^2 (approximately 6.7 η_q^2 in the physical world) are considered hereafter, to account for experimental noise. The origin of the holes in a turbulent flow is either (i) within the flow itself due to the internal intermittency of the velocity and scalar field or (ii) due to the large-scale entrainment (engulfment) of the ambient fluid. Without a Lagrangian approach, it is difficult to determine whether the scalar holes originate from the internal mechanics of the turbulence or are drawn into the primary shear flow from the surrounding environment. A methodology akin to that of Xu *et al.* (2023) is therefore adopted to distinguish the engulfed holes from those generated within the shear flow. Specifically, the concentration homogeneity within the scalar holes is investigated as a function of the Euclidean distance of their centroids to the interface, d_h. The r.m.s. concentration within the hole is defined as

$$\phi_h^{rms} = \sqrt{\overline{(\phi-\phi_h)^2}}, \qquad (3)$$

where ϕ_h represents the mean concentration within the hole. The ambient and the jet regions are characterized by low and high levels of concentration fluctuations, respectively. Hence, it is reasonable to anticipate that the engulfed holes, which are 'trapped' in the jet by large-scale events near the interface, possess relatively low ϕ_h^{rms}. Figure 4(*a*) presents the variation of ϕ_h^{rms} with distance from the TNTI and TTI outlines. Analogous to the velocity field (Xu *et al.* 2023), the scalar field inside the holes is initially uniform and gradually becomes inhomogeneous as the hole is positioned deeper into the shear flow. This trend is captured in figure 4(*a*), in which the scalar holes are divided into two regions with $d_{h-thre} \approx 0.08b_\phi$ as the border for all cases. Interestingly, $0.08b_\phi$ is very close to the thickness of the scalar interfacial layer for values of $\zeta = \mathcal{O}(0.1)$ (the inset of figure 3*d*), indicating that the behaviour of holes within the interfacial layer is essentially different from those in the turbulent core region (e.g. Jahanbakhshi & Madnia 2016). The probability density function (p.d.f.) of the characteristic length of the holes, $A_h^{1/2}$, in the two regions is displayed in figure 4(*b*), where it is found that the p.d.f.s inside the turbulent core (filled markers) appear to follow the -3 power-law. This scaling was previously reported by da Silva *et al.* (2014*b*) in direct numerical simulation of homogeneous isotropic turbulence (HIT), in which all the holes originate from the internal turbulence. We thus infer that holes with $d_h > 0.08b_\phi$ are statistically similar to those in HIT, and most likely not related to engulfment. On the other hand, the distribution of the p.d.f.s within the interfacial layer (hollow markers) is closer to a -5 power-law. This result falls between the -4 power-law distribution in a Mach-0.2 shear layer (Jahanbakhshi & Madnia 2016) and the -6 power-law distribution in an incompressible jet (Xu *et al.* 2023) observed for the p.d.f. of the characteristic size of the holes within the interfacial layer. This evidence suggests that holes with $d_h < 0.08b_\phi$ are likely engulfed by the large-scale motions of the jet.

Table 1 shows that ambient turbulence increases the relative area of the holes within the jet, despite a larger jet area. However, this does not necessarily indicate that engulfment is increased in the turbulent ambient, as only holes with $d_h < 0.08b_\phi$ are related to the engulfment, per the discussion above. The contribution of the engulfed mass flux to the total

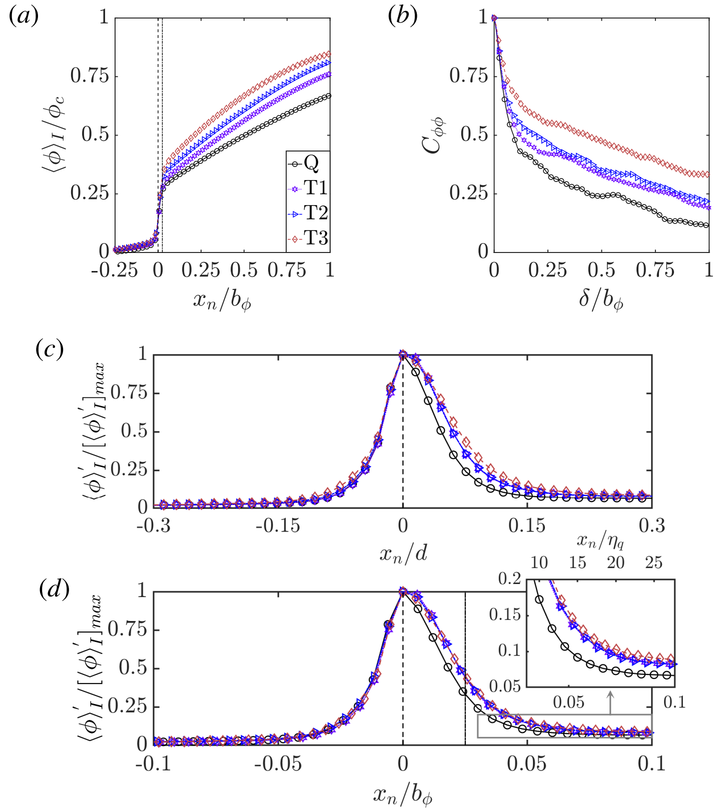

Figure 3. (*a*) Conditionally averaged profiles of mean concentration. (*b*) Conditional cross correlation function with probe at $x_n/b_\phi = 0.025$. (*c,d*) Gradient of the conditional profiles in (*a*) along the interface-normal coordinates. Note that the abscissas in (*c*) and (*d*) are non-dimensionalized with the jet-exit diameter, d, and scalar half-width, b_ϕ, respectively. The TNTI and TTI outlines ($x_n = 0$) are shown with the vertical dashed black line, while the vertical dashed-dotted line in (*a,d*) denotes the location of the probe for correlation profiles. The top x-axis in the inset of (*d*) is normalized by η_q.

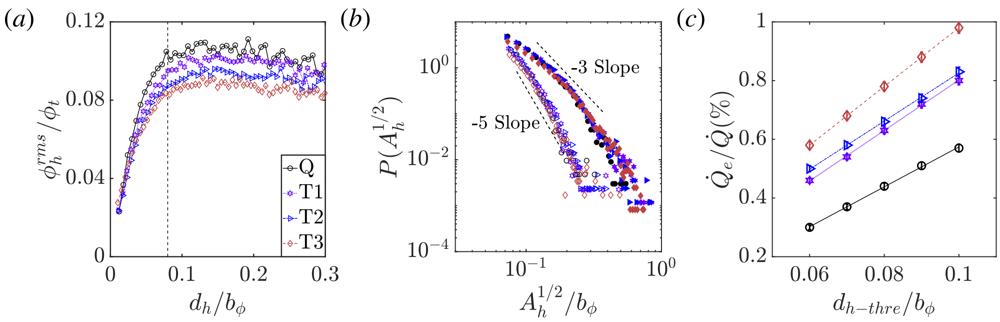

Figure 4. (*a*) Conditionally averaged profiles of r.m.s. concentration within the holes, normalized by the scalar thresholds that detect the interfaces. (*b*) P.d.f. of the characteristic length of the holes within the interfacial layer ($d_h < 0.08b_\phi$, hollow markers) and inside the turbulent region ($d_h > 0.08b_\phi$, filled markers). (*c*) Sensitivity of the assessed engulfed flux against the demarcation line, d_{h-thre}. The lines and error bars in (*c*) denote the best linear regression fit and the 95% confidence interval, respectively.

flux is estimated using (Westerweel *et al.* 2009),

$$\frac{\dot{Q}_e}{\dot{Q}} \approx \frac{2\pi\rho u_c \int_0^\infty \mathscr{P}_e(r)\, r\, \mathrm{d}r}{2\pi\rho u_c \int_0^\infty \mathscr{P}(r)\, r\, \mathrm{d}r}, \tag{4}$$

where, ρ, u_c, and $r = (y^2+z^2)^{1/2}$ denote the density, ensemble-averaged centerline velocity, and radial coordinate, respectively. Furthermore, $\mathscr{P}(r)$ represents the probability for a given fluid element in location r to be bounded by the outline, while $\mathscr{P}_e(r)$ is the probability for a given element to be a hole whose distance to the interface is less than d_{h-thre}. The ratio $\dot{Q}_e/\dot{Q}$ amounts to (0.44 $\pm$ 0.010)%, (0.63 $\pm$ 0.012)%, (0.66 $\pm$ 0.013)%, and (0.78 $\pm$ 0.015)% for cases Q, T1, T2, and T3, respectively, using $d_{h-thre} = 0.08b_\phi$. This result indicates that the contribution of engulfment is indeed increased in background turbulence, albeit slightly. Nibbling, or a third mechanism such as increased turbulent diffusion, appear to remain the dominant entrainment process in the far field of a jet, at least with the moderate background turbulence intensities investigated herein. The robustness of the engulfment flux estimation is illustrated in figure 4(*c*), where it is seen that variations of $\pm$25% in d_{h-thre} do not affect the aforementioned conclusion, that is, external turbulence promotes large-scale

Table 1. The averaged ratio of holes' and islands' area to that of the main jet for different cases. The averaged area of the jet (A_j) is also provided. Note that A_j is calculated as the area enclosed by the TNTI and TTI outlines, including the holes.

Case	A_j/d^2 (A_j/b_ϕ^2)	A_h/A_j (%)	A_i/A_j (%)
○ Q	51.6 (8.1)	1.55	4.36
✡ T1	59.8 (8.8)	1.99	8.53
▷ T2	61.8 (8.9)	2.06	9.21
◊ T3	88.1 (10.2)	2.78	11.85

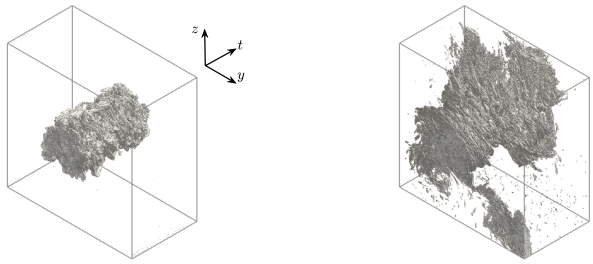

Figure 5. (2+1)-D space-time visualization of isosurface of ϕ_t for the jet in case Q (left panel) and case T3 (right panel). The cubes represent the spatial extent of the FOV.

engulfment in a jet.

Islands are defined as patches of scalar with $\phi \geqslant \phi_t$, which appear disconnected from the main jet region in our planar measurements. Table 1 reveals that external turbulence results in an increased contribution of the islands' area to that of the jet, noting that the ratio A_i/A_j is arguably underestimated in the turbulent ambient due to the extensive range of the islands and the limited size of the FOV (see, e.g., figure 1*b*). An increased occurrence of detached islands can be cautiously interpreted as strong local detrainment events, since the vortical structures containing the passive scalar are breaking away from the interface. The current experimental limitations may, however, complicate the identification of the genuine detrainment patches. Essentially, the detected islands may be attached to the jet region in a different streamwise plane through 3-D re-connection events, e.g., in the form of a 'tea-cup handle'. This is particularly an issue in the turbulent background due to the increased topological irregularities of the interface. We, therefore, use experimental visualizations to aid our narrative. In a quiescent ambient, the islands are usually re-entrained into free-shear flows and boundary layers within a few eddy turnover times (Westerweel *et al.* 2009). This is evident in figure 1(*a*), as the islands in the quiescent ambient are generally close to the TNTI outline. In a turbulent ambient, however, the islands are located further away from the jet and diffuse faster into the background (as seen in the experiments; also figure 1*b*), hindering the possibility of re-entrainment. Figure 5 shows (2+1)-D space-time visualizations of the jet for cases Q and T3 at the isocontours defined by the concentration threshold, ϕ_t. This has been achieved by stacking 526 contiguous PLIF snapshots, similar to Shan & Dimotakis (2006). It is worth noting that the evolution of the jet with downstream distance is not captured in figure 5, as the third dimension is essentially time. The present space-time data are, nonetheless, valuable for our purposes as they clearly demonstrate the large- and small-scale undulations of the interface and the intense detrainment events in the presence of external turbulence.

Compared to a non-turbulent ambient, the jet in external turbulence detrains more frequently due to the competition between the jet and background turbulence to entrain fluid from one another. When the TTI outline propagates towards the jet core (i.e. detrainment), large patches of passive scalar are left in the ambient. In the absence of a strong entrainment wind, these patches disperse from the interface and diffuse in the ambient by the action of turbulent eddies. The latter aligns with the concept of increased effective eddy diffusivity in the turbulent background, and suggests an increase in local detrainment events as compared to the quiescent ambient. This description also supports the hypothesis of Westerweel *et al.* (2009) regarding increased detrainment in external forcing and also the findings of Kankanwadi & Buxton (2020), who noticed extreme detrainment events for a wake in free-stream turbulence.

Consistent with the above description, Khorsandi *et al.* (2013) showed that external turbulence generated by the RJA tends to lower the entrainment into the far field of the jet. This notion is corroborated by investigating the radial profiles of the concentration skewness, defined as

$$S_\phi = \frac{\overline{(\phi - \overline{\phi})^3}}{[\overline{(\phi - \overline{\phi})^2}]^{3/2}}. \tag{5}$$

In the context of scalar entrainment, positive S_ϕ implies that fluid parcels containing the passive scalar are being mixed in a background of un-dyed fluid ($\phi > \overline{\phi}$ on average), whereas negative skewness suggests mixing of low-concentration patches within the shear flow, that is, $\phi < \overline{\phi}$ on average. Therefore, S_ϕ can act as a suitable surrogate for net entrainment into the jet. Figure 6 shows the effect of ambient turbulence on the scalar skewness of an axisymmetric jet. Prior to interpreting the results, we note that the skewness profile in the quiescent ambient shows good agreement with temperature measurements of Mi *et al.* (2001), indicating that the current experimental resolution accurately captures the third order scalar statistics. In a non-turbulent ambient, the value of S_ϕ is always negative at the centre of fully developed shear flows due to the entrainment of low-concentration background parcels. This trend also persists for the jet in our turbulent ambient cases (figure 6*a*) but, more importantly, the less negative values of S_ϕ within the core ($r/b_\phi \lesssim 1$) hint at the lowered entrainment into the jet. It is also worth mentioning that strong but sporadic meandering events in the turbulent ambient can even displace the jet center in space, causing artificially negative S_ϕ. This in turn leads to the overestimation of the entrained ambient parcels as inferred from the skewness profiles. This is addressed in figure 6(*b*), where the zonal average of scalar skewness within the jet, $S_{\phi_J} = \overline{(\phi - \overline{\phi_J})^3_J}/[\overline{(\phi - \overline{\phi_J})^2_J}]^{3/2}$, is presented along with the intermittency factor, γ, to show the effect of external intermittency due to meandering. The zonal average of quantity $\mathscr{C}$ is defined as $\overline{\mathscr{C}_J} = \overline{I\mathscr{C}}/\overline{I}$, where I is the intermittency function, set to zero in the ambient and to unity in the jet, so that $\gamma = \overline{I}$. It is appreciated that the values of S_{ϕ_J} remain closer to the Gaussian value of 0, owing to the removal of external intermittency by zonal sampling. Compared to S_ϕ, the profiles of S_{ϕ_J} in the turbulent ambient deviate further from their quiescent counterpart for $r/b_\phi \lesssim 1$, and better portray the effect of external forcing on the distribution of the scalar field within the jet. In summary and in accordance with the increased detrainment events, the

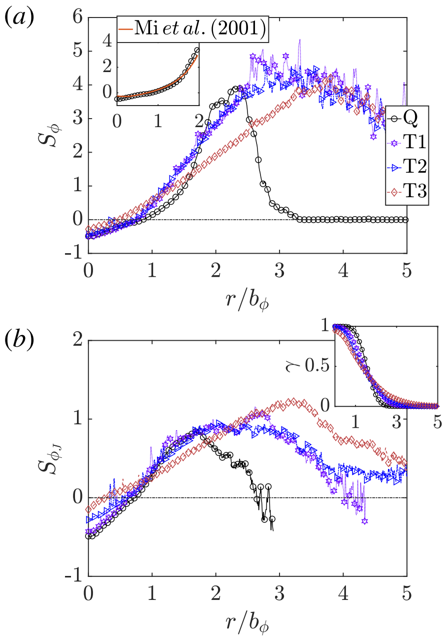

Figure 6. (a) Radial profiles of the scalar skewness for the studied cases. The inset displays S_ϕ in the quiescent ambient and that of Mi *et al.* (2001) at $x/d = 25$. (b) Zonal average of the scalar skewness within the jet. The inset shows the effect of external turbulence on the intermittency factor, γ.

results of figure 6 imply that the net entrainment of ambient fluid is suppressed in the presence of external turbulence.

CONCLUSIONS

Figure 7 summarizes the effect of ambient turbulence on the interfacial properties and entrainment into an axisymmetric jet. The action of external turbulence is to increase the large- and small-scale modulations of the interface (Kohan & Gaskin 2022) and to increase the thickness of the scalar interfacial layer. The two-point statistics revealed enhanced radial scalar transport towards the edges of the jet in the turbulent ambient, owing to increased turbulent diffusion and mean radial velocities (Khorsandi *et al.* 2013). Whilst external turbulence reduces the magnitude of the entrainment wind by disrupting the large eddying motions of the jet (Hunt 1994), the contribution of engulfment to the total mass flow rate is slightly enhanced (although still below 1%), seen as an increased presence of ambient holes within the finite thickness of the interfacial layer. This phenomenon can be potentially explained as the increased entrapment of low-concentrated ambient fluid elements between the inward cusps of the TTI outline.

The current planar visualizations showed that turbulence in the ambient results in an increased occurrence of concentration islands far away from the jet outline. This hints at local detrainment episodes due to the competition between the turbulent ambient and the jet to entrain fluid from one another, and can result in a reduced entrainment rate into the jet, despite a larger interfacial surface area. In accordance with the previous observation, the radial scalar skewness profiles also elucidated that mixing of ambient fluid inside the jet is restrained in the turbulent ambient. The present qualitative experimental approach pertaining the detrained patches may shed light on the detrainment mechanism in other turbulent flows and for other background conditions.

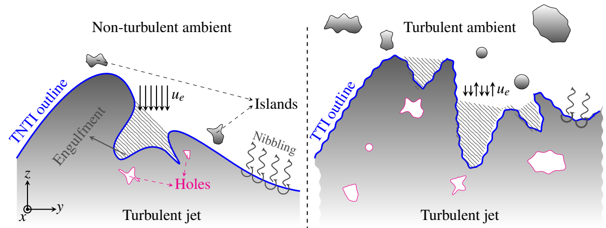

Figure 7. Conceptual model of the behaviour of the outer jet region in the presence of ambient turbulence. Note that u_e denotes the entrainment wind, induced by the large-scale motions of the jet. The hatched regions represent entrapment (engulfment) of ambient fluid.

REFERENCES

Friehe, C. A., van Atta, C. W. & Gibson, C. H. 1971 Jet turbulence: dissipation rate measurements and correlations. *AGARD Turbul. Shear Flows* **18**, 1-7.

Gaskin, S. J., McKernan, M. & Xue, F. 2004 The effect of background turbulence on jet entrainment: an experimental study of a plane jet in a shallow coflow. *J. Hydraul. Res.* **42** (**5**), 533-542.

Gladstone, C. & Woods, A. W. 2014 Detrainment from a turbulent plume produced by a vertical line source of buoyancy in a confined, ventilated space. *J. Fluid Mech.* **742**, 35-49.

Hunt, J. C. R. 1994 Atmospheric jets and plumes. In *Recent Research Advances in the Fluid Mechanics of Turbulent Jets and Plumes*, 309-334. Springer.

Jahanbakhshi, R. & Madnia, C. K. 2016 Entrainment in a compressible turbulent shear layer. *J. Fluid Mech.* **797**, 564-603.

Kankanwadi, K. & and Buxton, O. R. H. 2020 Turbulent entrainment into a cylinder wake from a turbulent background. *J. Fluid Mech.* **905**, A35.

Khorsandi, B., Gaskin, S. & Mydlarski, L. 2013 Effect of background turbulence on an axisymmetric turbulent jet. *J. Fluid Mech.* **736**, 250–286.

Kohan, K. F. & Gaskin, S. 2020 The effect of the geometric features of the turbulent/non-turbulent interface on the entrainment of a passive scalar into a jet. *Phys. Fluids* **32** (9), 095114.

Kohan, K. F. & Gaskin, S. J. 2022 On the scalar turbulent/turbulent interface of axisymmetric jets. *J. Fluid Mech.* **950**, A32.

Mi, J., Nobes, D. S. & Nathan, G. J. 2001 Influence of jet exit conditions on the passive scalar field of an axisymmetric free jet. *J. Fluid Mech.* **432**, 91-125.

Sahebjam, R., Kohan, K. F. & Gaskin, S. 2022 The dynamics of an axisymmetric turbulent jet in ambient turbulence interpreted from the passive scalar field statistics. *Phys. Fluids* **34** (1), 015129.

Shan, J. W. & Dimotakis, P. E. 2006 Reynolds-number effects and anisotropy in transverse-jet mixing. *J. Fluid Mech.* **566**, 47-96.

da Silva, C. B., Hunt, J. C. R., Eames, I. & Westerweel, J. 2014*a* Interfacial layers between regions of different turbulence intensity. *Ann. Rev. Fluid Mech.* **46**, 567-590.

da Silva, C. B., Taveira, R. R. & Borrell, G. 2014*b* Characteristics of the turbulent/nonturbulent interface in boundary layers, jets and shear-free turbulence. *J. Phys.: Conf. Ser.* **506** (1), 012015.

Westerweel, J., Fukushima, C., Pedersen, J. M. & Hunt, J. C. R. 2009 Momentum and scalar transport at the turbulent/non-turbulent interface of a jet. *J. Fluid Mech.* **631**, 199-230.

Wu, X., Wallace, J. M. & Hickey, J. P. 2019 Boundary layer turbulence and freestream turbulence interface, turbulent spot and freestream turbulence interface, laminar boundary layer and freestream turbulence interface. *Phys. Fluids* **31** (4), 045104.

Xu, C., Long, Y. & Wang, J. 2023 Entrainment mechanism of turbulent synthetic jet flow. *J. Fluid Mech.* **958**, A31.

You, J. & Zaki, T. A. 2019 Conditional statistics and flow structures in turbulent boundary layers buffeted by free-stream disturbances. *J. Fluid Mech.* **866**, 526-566.